PET-Based Radiation Dosimetry in Man of ^{18}F-Fluorodihydrotestosterone, a New Radiotracer for Imaging Prostate Cancer

Pat B. Zanzonico, PhD[1]; Ronald Finn, PhD[1]; Keith S. Pentlow, MS[1]; Yusuf Erdi, DSc[1]; Bradley Beattie, MS[1]; Timothy Akhurst, MD[1]; Olivia Squire, BA[1]; Michael Morris, MD[1]; Howard Scher, MD[1]; Timothy McCarthy, PhD[2]; Michael Welch, PhD[2]; Steven M. Larson, MD[1]; and John L. Humm, PhD[1]

[1]*Memorial Sloan-Kettering Cancer Center, New York, New York; and* [2]*Washington University, St. Louis, Missouri*

16β-fluoro-5α-dihydrotestosterone (FDHT) is a promising new PET radiopharmaceutical for the imaging of prostate cancer. A recent clinical trial provided the opportunity for refinement of normal-tissue radiation-absorbed dose estimates based on quantitative PET. The objective of the current study was to derive estimates of normal-tissue absorbed doses for ^{18}F-FDHT administered to patients with advanced prostate cancer. **Methods:** Absorbed dose estimates were derived from 10 ^{18}F-FDHT PET studies (administered activity, 111–407 MBq) of 7 prostate cancer patients. Activity concentrations in plasma and red marrow (assuming a plasmacrit of 0.58, an extracellular fluid fraction of 0.40, and equilibration of activity between plasma and marrow extracellular fluid) were measured ex vivo from a peripheral blood sample. Liver, spleen, urinary bladder contents, and total-body activities were measured by region-of-interest analysis of quantitative whole-body studies acquired with a dedicated PET scanner. Total organ activities and residence times were calculated from the respective PET scan–derived activity concentrations assuming standard (70 kg) man organ masses. Urinary excretion was corrected for hepatobiliary excretion (liver activity), and a first-order adjustment was made for the bladder-wall mass based on the patient's total-body mass. Mean organ absorbed doses were calculated with the MIRD formalism and the standard man model using the MIRDOSE3 software program. **Results:** The absorbed doses (mean ± SD) ranged from 0.00057 ± 0.000281 cGy/MBq (to skin) to 0.00868 ± 0.00481 cGy/MBq (to bladder wall) (voiding intervals, 1–2 h), and the effective dose equivalent was 0.00177 ± 0.000152 cSv/MBq. **Conclusion:** The maximum absorbed dose among all tissues in all 10 studies, 0.0151 cGy/MBq, occurred for the urinary bladder wall (with hydration and 1- to 2-h voiding intervals). To ensure that the maximum normal-tissue absorbed dose is kept below the recommended maximum permissible dose of 5 cGy per single administration, a maximum administered activity of 331 MBq (5 cGy/[0.0151 cGy/MBq]) is recommended for ^{18}F-FDHT.

Key Words: FDHT; dosimetry; prostate cancer; ^{18}F; androgens

J Nucl Med 2004; 45:1966–1971

Received Mar. 24, 2004; revision accepted May 5, 2004.

For correspondence or reprints contact: Pat Zanzonico, PhD, Memorial Sloan-Kettering Cancer Center, 1275 York Ave., New York, NY 10021.

E-mail: zanzonip@mskcc.org

Prostate cancer is one of the most important cancers in men in terms of both incidence and mortality, with more than 40,000 deaths per year in the United States (*1,2*). Prostate cancer exhibits a complex, temporally varying natural history (*3–6*), and metastatic prostate cancer is difficult to treat effectively. Virtually 100% of prostate cancer will initially respond to androgen withdrawal, but the tumor will subsequently alter its biology, becoming castration resistant and continuing to grow despite ongoing androgen suppression (*7,8*). The androgen receptor may therefore play a key role in the biologic behavior of prostate cancer. For this reason, PET of androgen receptors, especially in the patient whose disease is progressing despite low androgen levels, may be highly revealing.

16β-Fluoro-5α-dihydrotestosterone (FDHT) is a structural analog of 5α-dihydrotestosterone, the principal intraprostatic form of androgen. Among fluorinated androgen analogs studied in animals, FDHT uptake in the prostate was blocked (reduced ~10-fold) by coadministration of cold testosterone and yielded the highest levels of unmetabolized radioligand in blood up to 45 min after injection and the highest prostate-to-bone and prostate-to-muscle activity concentration ratios up to 4 h after injection (*9,10*). Thus, FDHT appears to bind specifically to androgen receptors in vivo and to have the most favorable targeting properties for noninvasive imaging among receptor-binding radiotracers studied to date. In addition, like androgens generally, most of the FDHT in circulation is bound to sex-hormone–binding globulin (*9,10*). Such plasma-protein binding presumably serves to retard degradation of endogenous androgens and to facilitate their transport into cells.

We have performed a study of 7 patients with progressive androgen-independent prostate cancer; the clinical results of that study have been presented in a separate article (*11*). In the current study, we describe the results of an assessment of the normal-tissue radiation

dosimetry derived from quantitative PET of this cohort of patients.

MATERIALS AND METHODS

Preparation of ^{18}F-FDHT

^{18}F-FDHT was prepared as previously described (*12*), starting with cyclotron-produced aqueous ^{18}F-fluoride, purified by normal-phase high-pressure liquid chromatography, evaporated to dryness, redissolved in ethanolic normal saline, and sterile-filtered for injection. The total radiochemistry synthesis time was 100 min, the specific activity greater than 22,200 GBq/mmol, the decay-corrected radiochemical yield nearly 30%, and the radiochemical purity, as determined by reverse-phase high-pressure liquid chromatography, greater than 95%.

Patients

A total of 10 ^{18}F-FDHT PET studies were performed on 7 patients with progressive prostate cancer. In all cases, the diagnosis of prostate cancer had been confirmed histologically and the progression of disease was confirmed by a standard bone scan, an abnormal CT or MRI scan, or rising serum titers of prostate-specific antigen. At the time of their respective studies, all subjects had serum levels of dihydrotestosterone, the active androgen in man, typical for prostate cancer patients after castration. Patients were injected intravenously with a bolus of 111–407 MBq of ^{18}F-FDHT.

Blood Sampling and Counting

Serial blood samples were obtained 0–60 min after injection via an indwelling venous catheter, weighed, and counted in a scintillation well counter calibrated for ^{18}F. Although exclusively blood-counting data were used for the dosimetric analysis, aliquots of some blood samples were also centrifuged and plasma decanted, weighed, and counted.

PET

A whole-body PET scan was obtained for each patient beginning at 66–154 min after injection using a dedicated PET scanner, the Advance (General Electric Medical Systems). The Advance is a bismuth germanate–based, multislice whole-body PET scanner with fields of view of 55 and 15 cm in the transaxial and axial directions, respectively. In the current study, all PET scans were obtained in 2-dimensional mode, yielding 35 transverse sections 4.25 mm in thickness over the 15-cm axial field of view. The nominal spatial resolution for ^{18}F is 4.2 mm in full-width at half-maximum in the transaxial plane (*13*). The Advance uses ^{68}Ge rods for a transmission-based attenuation correction; the whole-body emission scan was obtained first, requiring up to 7 bed positions per patient, and the ^{68}Ge transmission scans for the segmented attenuation correction were obtained immediately thereafter. Scatter and randoms corrections were applied using software provided with the scanner. The PET data were reconstructed by the ordered-subset expectation maximization iterative method to minimize the obscuring starburst artifact around intense foci of radioactivity (in this case, the urinary bladder) characteristic of filtered backprojection reconstruction.

Data Analysis

In the following analysis, all activities and activity concentrations were corrected for radioactive decay of ^{18}F from the time of the measurement/image (i.e., the start of the whole-body emission scan) back to the time of ^{18}F-FDHT injection. In addition, it was assumed that, as a first approximation, organ masses and compartment sizes (i.e., the extracellular fluid space) are directly proportional to total-body mass.

The maximum blood activity concentration was conservatively used to estimate the red marrow total activity. Assuming ^{18}F-FDHT instantaneously equilibrated between plasma and the red marrow extracellular fluid spaces, the maximum plasma and bone marrow activity concentrations were estimated from the maximum activity concentration among the serial blood samples using the following equation (*14*):

$$\text{Maximum marrow [activity]} = \frac{\text{Standard man red marrow ECF fraction, 0.40}}{\text{Standard man plasmacrit, 0.58}} \cdot \text{Maximum blood [activity]}, \quad \text{Eq. 1}$$

where maximum marrow [activity] = the maximum marrow activity concentration (in MBq/g) and maximum blood [activity] = the maximum blood activity concentration (in MBq/g). In Equation 1, the standard man red marrow extracellular fraction was taken as 0.40 (*15*) and plasmacrit as 0.58 (*16*). The maximum total marrow activity was then estimated as follows:

$$\text{Marrow total activity} = \frac{\text{Patient total-body mass}}{\text{Standard man total-body mass, 70 kg}} \cdot \text{Standard man marrow mass, 1,500 g} \cdot \text{Maximum marrow [activity]}. \quad \text{Eq. 2}$$

In Equation 2, the standard man total-body mass was taken as 70 kg and the standard man red marrow mass as 1,500 g (*16*).

Region-of-interest analysis was performed on the quantitative PET images, yielding the mean activity concentrations (in kBq/mL) in the liver, spleen, and total body. The total activity in organ i was then estimated using the following equation:

$$\text{Organ i total activity} = \frac{\text{Patient total-body mass}}{\text{Standard man total-body mass, 70 kg}} \cdot \text{Standard man organ i mass} \cdot \text{Organ i mean activity concentration}. \quad \text{Eq. 3}$$

The ^{18}F residence time τ_i in organ i (i.e., the liver, spleen, and red marrow) was conservatively calculated assuming elimination of activity only by physical decay in situ:

$$\tau_i = 1.44\, T_p \frac{\text{Organ i total activity}}{\text{Administered activity}}, \quad \text{Eq. 4}$$

where T_p = the physical half-life of ^{18}F, 1.8 h.

The ^{18}F residence time τ_{TB} in the total body was calculated from the total-body effective half-life of ^{18}F-FDHT, assuming monoexponential biologic clearance from the time of injection to the time of the PET scan:

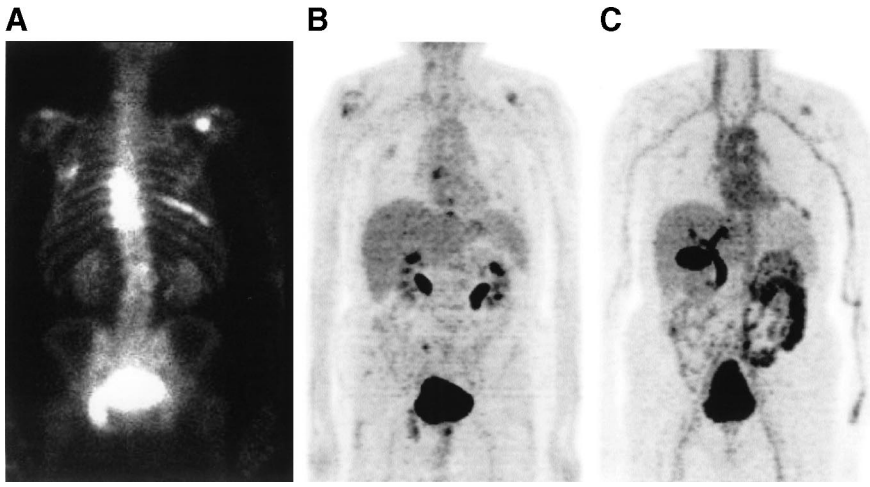

FIGURE 1. Comparative whole-body images of a 75-y-old man with progressive prostate cancer metastatic to bones of the thoracic spine, left rib cage, and scapula: planar γ-camera image of ^{99m}Tc-methylene diphosphonate (A); 1-pixel-thick coronal PET image of ^{18}F-FDG (B); and 1-pixel-thick coronal PET image of ^{18}F-FDHT (C).

$$\tau_{TB} = 1.44\, T_e \qquad \text{Eq. 5}$$

$$= 1.44\, \frac{T_p (T_b)_{TB}}{T_p + (T_b)_{TB}}, \qquad \text{Eq. 6}$$

where $(T_b)_{TB}$ = the biologic half-time of FDHT-derived ^{18}F in the total body.

The activity excreted up to the time of each PET scan was calculated from the total-body activity using the following equation:

$$\text{Activity excreted} = \text{Administered activity} - \text{Total-body activity}. \qquad \text{Eq. 7}$$

Assuming the activity in the liver at the time of each PET scan would be eliminated via hepatobiliary excretion, the fraction of the excreted activity excreted in the urine was estimated using the following equation:

$$\text{Fraction of excreted activity excreted in urine} = 1 - \text{Fraction of administered activity in liver}. \qquad \text{Eq. 8}$$

The ^{18}F residence times in the intestines (i.e., the small intestine, upper large intestine, and lower large intestine) were calculated on the basis of the assumption that the activity in the liver was eliminated entirely via hepatobiliary excretion, equating the fraction of the administered activity in the liver at the time of each PET scan with the fraction of the administered activity entering the small intestine and using the International Commission on Radiological Protection (ICRP) 30 gastrointestinal tract model (*17*) as implemented with the MIRDOSE3 software program (*18*). The ^{18}F residence time in the urinary bladder contents was calculated using the dynamic bladder model as implemented with the MIRDOSE3 software program (*18*), with the biologic half-time of FDHT-derived ^{18}F in the total body and the fraction of the excreted activity excreted in the urine (Eq. 7). Because not all of the activity in the liver may be excreted via the intestines, that is, some of the liver activity may ultimately be eliminated in the urine, the foregoing approach may overestimate the radiation dose to the intestines while underestimating that to the bladder wall.

Mean organ absorbed doses (in cGy/MBq administered) were calculated using S-factor values for the 70-kg standard man anatomic model and the MIRD formalism as implemented with the MIRDOSE3 software program (*18*). The effective dose equivalent was calculated assuming a radiation weighting factor of unity for ^{18}F radiation and using the ICRP 60 tissue weighting factors (*19,20*).

RESULTS

Imaging and Biodistribution Data

A PET image (coronal section) showing the typical whole-body distribution of ^{18}F-FDHT in a patient with metastatic prostate cancer is presented in Figure 1 C. For comparison, a planar γ-camera image of ^{99m}Tc-methylene diphosphonate and a coronal-section PET image of ^{18}F-FDG are shown in Figures 1A and 1B, respectively.

Based on region-of-interest analysis of the PET image data (10 studies in 7 patients), the decay-corrected percentage injected dose (mean ± SD) in the liver, spleen, and total body at 66–154 min after injection was 9.0% ± 4.3%, 0.82% ± 0.75%, and 78% ± 16%, respectively. The activity concentration in plasma rapidly reaches a maximum by ~2 min after injection and decreases by less than 30% up to 60 min after injection (Fig. 2). The decay-corrected maxi-

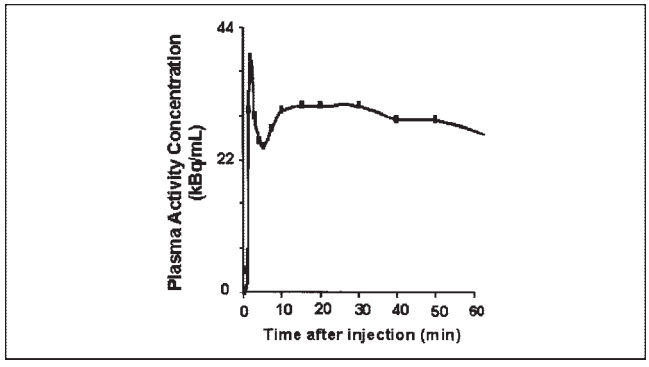

FIGURE 2. Typical plasma time–activity concentration curve for ^{18}F-FDHT through 60 min after injection. The activity concentrations, expressed in units of MBq/mL, have been decay-corrected back to the time of injection.

TABLE 1
Radiation Dosimetry of ^{18}F-FDHT in Prostate Cancer Patients

	Absorbed dose (cGy/MBq)												
	Patient 1	Patient 2		Patient 3		Patient 4		Patient 5	Patient 6	Patient 7			
Target organ	Study 1 248 MBg	Study 1 407 MBg	Study 2 189 MBg	Study 1 111 MBg	Study 2 281 MBg	Study 1 407 MBg	Study 2 407 MBg	Study 1 270 MBg	Study 1 396 MBg	Study 1 377 MBg	Mean	SD	% SD
Adrenals	0.00151	0.00126	0.00087	0.00156	0.00077	0.00085	0.00113	0.00099	0.00057	0.00132	0.00108	0.000329	30
Brain	0.00108	0.00066	0.00023	0.00107	0.00045	0.00050	0.00078	0.00042	0.00006	0.00086	0.00061	0.000341	56
Gallbladder wall	0.00165	0.00154	0.00131	0.00172	0.00092	0.00096	0.00123	0.00129	0.00074	0.00142	0.00128	0.000326	26
Lower large intestine wall	0.00143	0.00108	0.00078	0.00143	0.00096	0.00106	0.00134	0.00088	0.00041	0.00132	0.00107	0.000327	31
Small intestine	0.00148	0.00106	0.00063	0.00149	0.00079	0.00086	0.00119	0.00079	0.00032	0.00127	0.00099	0.000379	38
Stomach	0.00139	0.00095	0.00048	0.00139	0.00063	0.00069	0.00102	0.00070	0.00030	0.00118	0.00087	0.000375	43
Upper large intestine wall	0.00146	0.00107	0.00065	0.00148	0.00076	0.00083	0.00115	0.00080	0.00033	0.00125	0.00098	0.000369	38
Heart wall	0.00139	0.00099	0.00055	0.00141	0.00064	0.00069	0.00102	0.00072	0.00027	0.00115	0.00088	0.000374	42
Kidneys	0.00141	0.00109	0.00068	0.00143	0.00069	0.00076	0.00105	0.00084	0.00046	0.00123	0.00096	0.000328	34
Liver	0.00257	0.00457	0.00597	0.00303	0.00227	0.00218	0.00189	0.00465	0.00368	0.00249	0.00333	0.001344	40
Lungs	0.00125	0.00089	0.00049	0.00126	0.00057	0.00062	0.00091	0.00065	0.00025	0.00104	0.00079	0.000332	42
Muscle	0.00120	0.00082	0.00045	0.00120	0.00060	0.00066	0.00094	0.00060	0.00020	0.00101	0.00077	0.000324	42
Pancreas	0.00155	0.00121	0.00076	0.00157	0.00076	0.00082	0.00115	0.00097	0.00059	0.00139	0.00108	0.000350	32
Red marrow	0.00182	0.00231	0.00167	0.00221	0.00135	0.00184	0.00172	0.00171	0.00193	0.00216	0.00187	0.000293	16
Bone surfaces	0.00163	0.00166	0.00106	0.00184	0.00100	0.00131	0.00140	0.00119	0.00111	0.00169	0.00139	0.000300	22
Skin	0.00095	0.00061	0.00028	0.00095	0.00043	0.00047	0.00071	0.00042	0.00010	0.00078	0.00057	0.000281	49
Spleen	0.00179	0.00172	0.00038	0.00133	0.00116	0.00117	0.00140	0.00311	0.00673	0.00454	0.00233	0.001941	83
Testes	0.00117	0.00080	0.00051	0.00115	0.00071	0.00076	0.00103	0.00062	0.00020	0.00102	0.00079	0.000307	39
Thymus	0.00125	0.00080	0.00033	0.00125	0.00053	0.00058	0.00091	0.00053	0.00012	0.00101	0.00073	0.000378	52
Thyroid	0.00123	0.00075	0.00027	0.00123	0.00051	0.00056	0.00089	0.00048	0.00007	0.00098	0.00070	0.000391	56
Urinary bladder wall	0.00151	0.00659	0.01503	0.00106	0.01278	0.01338	0.01105	0.01038	0.00881	0.00616	0.00868	0.004808	55
Total body	0.00125	0.00096	0.00063	0.00127	0.00067	0.00074	0.00099	0.00074	0.00036	0.00109	0.00087	0.000292	34
Effective dose equivalent (cSv/MBq)	0.00152	0.00178	0.00201	0.00159	0.00170	0.00184	0.00188	0.00186	0.00165	0.00189	0.00177	0.000152	9

mum activity concentration in plasma through 60 min after injection was 0.0061% ± 0.0015%/mL.

Residence Times and Radiation Doses

The ^{18}F residence times in the liver, spleen, red marrow, and total body ranged from 0.15 to 0.46 h, 0.0077 to 0.063 h, 0.11 to 0.24 h, and 1.0 to 2.6 h, respectively. The mean normal-tissue absorbed doses (in cGy/MBq) and the effective dose equivalent (in cSv/MBq), with the respective SDs and percentage SDs, are presented in Table 1 for all 10 ^{18}F-FDHT studies. Except for the liver (0.00333 cGy/MBq) and the urinary bladder wall (0.00868 cGy/MBq), the mean absorbed dose to each tissue was less than 0.003 cGy/MBq. The effective dose equivalents ranged from 0.00152 to 0.00201 cSv/MBq. These absorbed doses, which provide the basis for the recommended administered activity of ^{18}F-FDHT (*21*), are comparable to those of other ^{18}F-labeled radiopharmaceuticals such as ^{18}F-FDG (*22*).

DISCUSSION

The current clinical study derived normal-tissue radiation dose estimates for a promising new radiotracer, ^{18}F-FDHT, for prostate cancer, based on quantitative whole-body PET and serial blood sampling in patients with progressing disease. A total of 10 whole-body PET scans were obtained for 7 patients. Certainly, measurement of normal-tissue time–activity data based on serial PET scans, rather than on only a single scan, would yield more reliable dose estimates. However, in our initial clinical studies with ^{18}F-FDHT (*11*), the primary objective was evaluation of tumor targeting rather than measurement of whole-body normal-tissue distribution and only a single whole-body scan was obtained. With further clinical application of ^{18}F-FDHT, we anticipate the opportunity to eventually acquire more complete kinetic data and thus refine our absorbed dose estimates. The current dose estimates are conservative, therefore, in that it was assumed that there was no biologic clearance from individual organs. The overestimation of tissue absorbed doses associated with this conservative assumption may be assessed on the basis of estimates of the total-body biologic and effective half-times of ^{18}F-FDHT. The decay-corrected total-body activities measured by PET from 66 to 154 min after injection ranged from 53% to ~100%, yielding total-body biologic half-times of 1 h to greater than 10 h and therefore effective half-times of 0.72 to 1.8 h; most of the effective half-times were in the 1.2- to 1.8-h range and the mean was 1.3 h. This suggests that our absorbed dose estimates for ^{18}F-FDHT, based on the assumption of no biologic clearance from individual organs, may overestimate the actual doses by an average of 38% (1.8/1.3 × 100% = 138%).

As noted, the ^{18}F residence times in the intestines were estimated assuming the activity in the liver was eliminated entirely via hepatobiliary excretion, equating the fraction of the administered activity in the liver at the time of each PET scan with the fraction of the administered activity entering the intestinal tract. This is, of course, a conservative assumption in that it maximizes the estimates of the intestinal residence times and absorbed doses, since some of the hepatic activity may not actually be excreted through the intestines but rather through the urinary bladder. This assumption may therefore also lead to somewhat of an underestimate of the urinary bladder residence time and absorbed dose. With the limited data available from the current study, however, it is not possible to reliably estimate the magnitude of these errors.

In the current study, the highest absorbed doses (mean ± SD) were delivered to the urinary bladder wall, 0.0.00868 ± 0.00481 cGy/MBq, and the liver, 0.00333 ± 0.00134 cGy/MBq. The radiation doses thus derived, including the effective dose equivalent (0.00177 ± 0.000152 cSv/MBq), were comparable to previous estimates for ^{18}F-FDHT determined in nonhuman primates (*9*).

CONCLUSION

Although not actually applicable to routine (i.e., noninvestigational) studies in patients, the maximum permissible dose limit of 5 cGy (rad) per study to normal tissues is a reasonable basis for specifying the administered activity for diagnostic studies with ^{18}F-FDHT. Based on a maximum absorbed dose of 0.0151 cGy/MBq to the urinary bladder wall among all tissues in all 10 studies, an administered activity of 5 cGy/(0.0151 cGy/MBq) = 331 MBq is recommended for diagnostic studies (*21*). This is comparable to administered activities routinely used for ^{18}F-labeled diagnostic agents such as ^{18}F-FDG (*22*).

ACKNOWLEDGMENTS

This work was supported in part by U.S. Department of Energy grants DE-FG02-86ER60407 and DE-FG02-84ER60218, the Hasco Foundation, and Pepsico.

REFERENCES

1. Jemal A, Murray T, Samuels A, et al. Cancer statistics, 2003. *CA Cancer J Clin.* 2003;53:5–26.
2. Horst T, Meyer B, Taplin S. Screening, health promotion, and prevention in men. *Prim Care.* 1995;22:679–695.
3. Fenton MA, Shuster TD, Fertig AM, et al. Functional characterization of mutant androgen receptors from androgen-independent prostate cancer. *Clin Cancer Res.* 1997;3:1383–1388.
4. Craft N, Sawyers CL. Mechanistic concepts in androgen-dependence of prostate cancer. *Cancer Metastasis Rev.* 1998;17:421–427.
5. Visakorpi T, Hyytinen E, Koivisto P, et al. In vivo amplification of the androgen receptor gene and progression of human prostate cancer. *Nat Genet.* 1995;9:401–406.
6. Koivisto P, Visakorpi T, Rantala I, et al. Increased cell proliferation activity and decreased cell death are associated with the emergence of hormone-refractory recurrent prostate cancer. *J Pathol.* 1997;183:51–56.
7. Agus DB, Cordon-Cardo C, Fox W, et al. Prostate cancer cell cycle regulators: response to androgen withdrawal and development of androgen independence. *J Natl Cancer Inst.* 1999;91:1869–1876.
8. Agus DB, Golde DW, Sgouros G, et al. Positron emission tomography of a human prostate cancer xenograft: association of changes in deoxyglucose accu-

mulation with other measures of outcome following androgen withdrawal. *Cancer Res.* 1998;58:3009–3014.
9. Bonasera TA, O'Neil JP, Xu M, et al. Preclinical evaluation of fluorine-18-labeled androgen receptor ligands in baboons. *J Nucl Med.* 1996;37:1009–1015.
10. Choe YS, Lidstrom PJ, Chi DY, et al. Synthesis of 11 beta-[^{18}F]fluoro-5 alpha-dihydrotestosterone and 11 beta-[^{18}F]fluoro-19-nor-5 alpha-dihydrotestosterone: preparation via halofluorination-reduction, receptor binding, and tissue distribution. *J Med Chem.* 1995;38:816–825.
11. Larson SM, Morris M, Gunther I, et al. Tumor localization of 16β-^{18}F-fluoro-5α-dihydrotestosterone versus ^{18}F-FDG in patients with progressive, metastatic prostate cancer. *J Nucl Med.* 2004;45:366–373.
12. Liu A, Dence CS, Welch MJ, et al. Fluorine-18-labeled androgens: radiochemical synthesis and tissue distribution studies on six fluorine-substituted androgens, potential imaging agents for prostatic cancer. *J Nucl Med.* 1992;33:724–734.
13. DeGrado TR, Turkington TG, Williams JJ, et al. Performance characteristics of a whole-body PET scanner. *J Nucl Med.* 1994;35:1398–1406.
14. Sgouros G. Bone marrow dosimetry for radioimmunotherapy: theoretical considerations. *J Nucl Med.* 1993;34:689–694.
15. Siegel J, Wessels B, Watson E, et al. Bone marrow dosimetry and toxicity in radioimmunotherapy. *Antibody Immunocon Radiopharm.* 1990;3:213–223.
16. International Commission on Radiological Protection. *Report of the Task Group on Reference Man.* Oxford, U.K.: Pergamon Press; 1975. ICRP publication 23.
17. International Commission on Radiological Protection. Limits for intakes of radionuclides by workers. In: *Annals of the ICRP.* Vol 2. Oxford, U.K.: Pergamon Press; 1979. ICRP publication 30 (part 1).
18. Stabin MG. MIRDOSE: personal computer software for internal dose assessment in nuclear medicine. *J Nucl Med.* 1996;37:538–546.
19. International Commission on Radiological Protection. *Radiation Dose to Patients from Radiopharmaceuticals.* New York, NY: Pergamon Press; 1988. ICRP publication 53.
20. International Commission on Radiation Units and Measurements. *Fundamental Quantities and Units for Ionizing Radiation.* Bethesda, MD: ICRU; 1998. ICRU report 60.
21. Food and Drug Administration. Part 361: prescription drugs for human use generally recognized as safe and effective and not misbranded—drugs used in research. Section 361.1: radioactive drugs for certain research purposes. In: *Code of Federal Regulations.* Washington, DC: U.S. Government Printing Office; 2000. 21 CFR Ch 1:298–302.
22. Jones SC, Alavi A, Christman D, et al. The radiation dosimetry of 2 [F-18]fluoro-2-deoxy-D-glucose in man. *J Nucl Med.* 1982;23:613–617.

snm
advancing molecular imaging